International Journal of Heat and Mass Transfer 52 (2009) 5141–5151

Contents lists available at ScienceDirect

International Journal of Heat and Mass Transfer

journal homepage: www.elsevier.com/locate/ijhmt

Development of a mesoscopic particle model for synthesis of uranium-ceramic nuclear fuel

Xiaolin Wang [a], Hui Zhang [b], Lili Zheng [a,c,*], Jiuan Wei [a]

[a] Department of Mechanical Engineering, Stony Brook University, Stony Brook, NY 11794, USA
[b] Department of Engineering Physics, Center for Public Safety Research, Tsinghua University, Beijing 100084, China
[c] School of Aerospace, Tsinghua University, Beijing 100084, China

ARTICLE INFO

Article history:
Received 12 February 2008
Received in revised form 16 April 2009
Accepted 16 April 2009
Available online 13 June 2009

Keywords:
Mesoscopic
Porous media
Synthesis
Smoothed particle hydrodynamics
Nuclear fuel

ABSTRACT

A novel technique has been developed to fabricate uranium-ceramic nuclear fuel using the depleted uranium (DU), U_3O_8 powder, and allylhydridopolycarbosilane (AHPCS) polymer precursor. This process involves a continuous change of the composition, porosity, and material properties. To fabricate nuclear fuel with a uniform structure/volume ratio, it is important to understand the transport phenomena during high temperature processing and at different length scales. In our prior work, a system-level model based on the reactive porous medium theory was developed to account for pyrolysis process during the uranium-ceramic fuel fabrication. In this paper, a mesoscopic model based on the smoothed particle hydrodynamics (SPH) is developed to simulate the synthesis of filler U_3O_8 particles and SiC matrix. The system-level model provides the necessary thermal boundary conditions for the mesoscopic simulation. The evolution of the particle concentration and the structure as well as the composition of the composite produced is investigated. Since the process heat flux plays an important role in the material quality and uniformity, the effect of the heating rate, filler particle size and distribution on the uniformity and the structure of the final product are investigated. The uncertainty issue is also discussed.

1. Introduction

A novel preparation technique for the nuclear fuels starting from the depleted uranium (DU), U_3O_8 powder, and allylhydridopolycarbosilane (AHPCS) polymer precursor has been developed in our prior study [1]. This processing cycle involves the curing of the polymer precursor mixed with the U_3O_8 particles at 150–250 °C, in which the polymer undergoes cross-linking to form a green body, followed by a pyrolysis stage which involves the formation of the amorphous SiC between 400 °C and 900 °C, the crystallization of SiC and the synthesis of SiC and U_3O_8 at 1000–1500 °C, UC can be produced in the synthesis. This processing technique allows the uniform distribution of the uranium fuel source along with a high ceramic yield of the parent matrix. The processing technique offers an inexpensive method to obtain a dense nuclear fuel. The resulting ceramic composite has the uranium oxide well dispersed in *a*-SiC matrix. The thermal conductivity of the composite can be improved through the crystallization owing to the high conductivity of SiC [2]. Further mechanical consolidation was achieved using the polymer infiltration process (PIP). Among various advanced ceramics, the silicon carbide has been proven to be a promising candidate for use in the nuclear applications as an inert-matrix material due to its characteristics in the following aspects. First, SiC displays a number of superior characteristics as a structural material, such as its thermal and mechanical properties, chemical stability and low radioactivation. Second, the irradiation effects on swelling and mechanical properties of high purity SiC have been evaluated, and the excellent high temperature irradiation resistance was revealed by several researchers [3,4]. Third, the SiC matrix composites have been widely developed for use in the advanced energy systems [5–7]. It has also been recognized that the uranium carbide (UC) is an attractive fuel for certain generation IV reactors such as the gas-cooled fast reactor due to its high thermal conductivity and high melting point. Therefore, the ceramic composite pellets consisting of the UC particles in the SiC matrix can be used as a high-temperature refractory ceramic fuel due to the superior characteristics of UC and SiC.

The pyrolysis and synthesis processing technique allows the fabrication of various ceramic materials at a relative low temperature. Also, it allows the fabrication of the net-shape components without suffering from the size limitation [8]. During the powder synthesis, the powder binding mechanism strongly depends on the local temperature and heat flux. Meanwhile, the morphological changes at the particle scale will influence the thermal transport and in turn, affect the local temperature. Several numerical models have been developed, which can be generally categorized into two approaches: the porous media based approach and the particle

* Corresponding author. Address: Department of Mechanical Engineering, Stony Brook University, Stony Brook, NY 11794, USA. Tel./fax: +86 10 62797961.
E-mail address: zhenglili@tsinghua.edu.cn (L. Zheng).

0017-9310/$ - see front matter © 2009 Elsevier Ltd. All rights reserved.
doi:10.1016/j.ijheatmasstransfer.2009.04.028

Nomenclature

C_p	Specific heat at constant pressure (J/Kg K)
D	Diffusivity (m^2/s)
D	Particle diameter (m)
F	Volume ratio
k_s	Thermal conductivity (W/m K)
r_{ij}	Distance between particle i and j (m)
m	Mass (kg)
$\dot{m}$	Mass generation rate (kg/s)
N	Number of particles at the neighboring
P	Gases products
q''	Heat flux (W/m^2)
$\dot{Q}$	Reaction heat (kg/s)
T	Temperature (K)
t	Time (s)
$\vec{u}$	Velocity vector (m/s)
W	Smoothing function
Y	Mass fraction
$\dot{Y}$	Generation rate of mass fraction

Greek symbols

α	Coefficient
ρ	Density (kg/m^3)
μ	Viscosity (kg/m s)
ν	Kinematics viscosity (m^2/s)

Subscripts

1	SiC
2	Filler particles
g	Gas phase
i	Particle i
j	Particle j
s	Solid phase
β	Coordinate direction

based approach. The porous media based approach is based on the porous media theory to describe the macroscopic property evaluation during the synthesis or sintering process. Tarafdar and Bergman [9] developed a sintering model to investigate the variations of the local morphologies on the effective transport properties. They found that the penetration depth of the sintering was strongly related to the thermal penetration depth and boundary temperatures. Chen and Zhang [10] developed a partial shrinkage model for the selective laser sintering (SLS) of two-component metal powder and they discovered that the sintering depth and volume of the HAZ was significantly increased with the decrease of the gas volume fraction. Xiao and Zhang [11] studied the melting of an alloy powder bed. It was concluded that the increase of the initial porosity of the powder bed can shorten the duration of the preheating and increase the surface temperature and interfacial velocity. He et al. [12] presented a model to study the effects of the particle convection, gas convection and radiation. They concluded that the radiative heat transfer provided a significant contribution to the total heat transfer, and the particle and gas convections show an opposite tendency to the total heat transfer. Kaushal et al. [13] developed a model for the biomass char combustion in a fluidized bed. It is shown that a smaller size of wood or char benefits the overall performance of the gasifier.

Several particle based models are developed for mesoscopic phenomena in the materials processing or underground water flow focusing on the local behaviors around the particles and studying the evolution of the structure and the heat and mass transfer on the particle level. Jagota and Dawson [14] and Martinez-Herrera and Derby [15] used the finite element methods (FEM) to study the shape evolution of the adjacent sintering particles. The effect of particle geometry on the sintering rate is also investigated. It was concluded that the assumption of spherical particle shape is reasonable to predict sintering dynamics for many different particle geometries. He et al. [12] proposed a one dimensional char combustion model considering the pore structure to investigate the effect of the particle size on the transport phenomena in the single char combustion. The simulation results show that the larger particles generally have higher temperatures at the exterior surface, and the smaller particles have the better combustion efficiency in a limited period. Gao et al. [16] presented a double particle-layer and porous medium model to simulate the gas flow and the heat transfer near the surface of an immersed object in a fluidized bed. They concluded that the heat transfer rate is determined by the gas velocity. The heat transfer is conduction dominated in the stifling region since the gas is almost stagnant there. Tartakovsky and Meakin developed a numerical model to simulate the multiphase flows and the miscible flows in the fractured porous media using the meshless particle SPH method [17]. The effects of the pore level heterogeneity and anisotropy on the immiscible and miscible flows were studied [17]. Tartakovsky et al. [18] further improved their model to study the reactive transport and the mineral precipitation in the porous media. They concluded that the initial perturbation of the solid surface leaded to the unstable growth and the increase of the reaction length parameter can stabilize the non-uniform surface growth.

A macroscopic model for the pyrolysis processing was developed in our prior work [19] in which the Darcy's law and the convection–diffusion equations were used to model the volatile flow in the porous media. The system-level or global model describes the polymer pyrolysis processing, including heat transfer, polymer pyrolysis, SiC crystallization, chemical reactions, and volatiles transport. However, the modeling the particle level structure evolution of the composite produced during synthesis of the uranium oxide and SiC is needed for the process optimization. In this paper, a mesoscopic model is developed based on the meshless particle method to study the structure and species evolution at the mesoscopic or local level. The mesoscopic model is applied to a repetitive unit cell and describes the mass transport, the composition change and the movement of the particles. The unit cell represents a unit of the source material that consists of several U_3O_8 particles, the SiC matrix and other components produced from synthesis. The smoothed particle hydrodynamics (SPH) technique is employed to solve the solid–solid reaction between the SiC matrix and the filler particles, the composition changes, the uniformity of the resulting products, and the shrinkage and the motion of the U_3O_8 particles in the SiC matrix. The results from the macroscale simulation are used to provide the necessary thermal boundary conditions for the particle level simulations. The evolution of the structure and the composition of the produced composite due to the heat fluxes are monitored. The effects of the heating rate and the U_3O_8 particle size and volume on the species uniformity and the structure formation are investigated. The uncertainty due to the random distribution of the filler particles is also investigated.

2. Physical and mathematical model

Fig. 1 shows the key elements of the SPH local model within a macro computation domain that is constituted by many

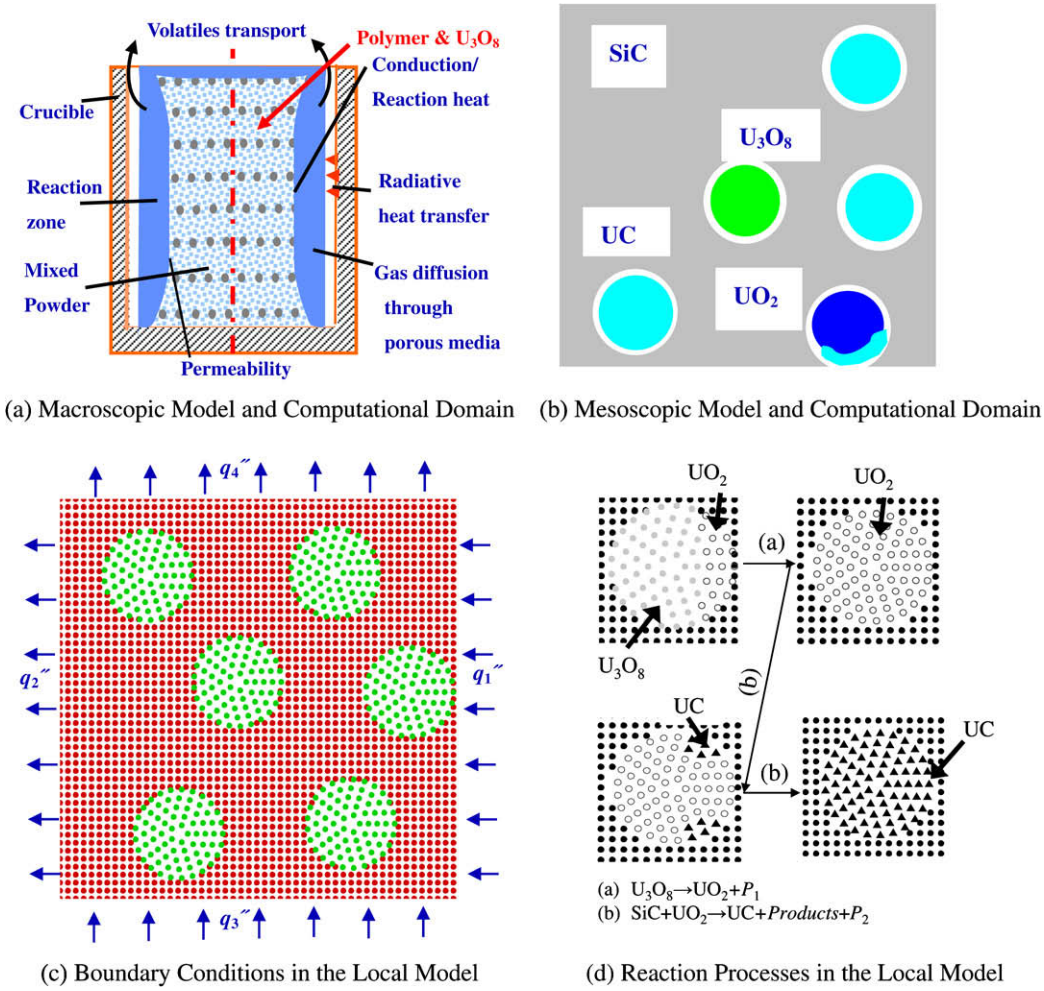

(a) Macroscopic Model and Computational Domain (b) Mesoscopic Model and Computational Domain

(c) Boundary Conditions in the Local Model (d) Reaction Processes in the Local Model

Fig. 1. The schematic of the SPH local model and its interaction with the global porous medium model.

macrocells. Each macrocell is a representative unit of the source material, and it consists of several U_3O_8 particles, SiC matrix and other components produced from the synthesis process. The mesoscopic particle-level model applies to a repetitive macrocell unit for the microstructure evolution calculation. The temperature boundary condition for the chosen marcocell can be obtained from its neighbor cells by interpolating the nearest neighbor macrocell temperature to the boundary. In the current system, the governing equations at the particle level can be described as follows,

$$\text{The continuity equation}: \quad \frac{\partial \rho}{\partial t} + \nabla \cdot (\rho \vec{u}) = \dot{m} \tag{1}$$

$$\text{The energy equation}: \frac{\partial}{\partial t}(\rho c_p T) + \nabla \cdot (\rho c_p \vec{u} T) = \nabla \cdot (k \nabla T) + \dot{Q} \tag{2}$$

$$\text{The species equation}: \frac{\partial Y}{\partial t} + \nabla \cdot (\vec{u} Y) = \frac{1}{\rho} \nabla \cdot (D \nabla Y) + \dot{Y}, \tag{3}$$

where ρ, c_p and κ are the density, specific heat and thermal conductivity, respectively; $\dot{Y}$ is the mass fraction, and D is the diffusion coefficient. In the local model, the matrix SiC is stationary and the filler particles move due to the generated gas pressure, and $\dot{m}$, $\dot{Q}$ and $\dot{Y}$ are the source terms due to the chemical reactions. The transient heat fluxes obtained from the global model are applied as the thermal boundary conditions.

In the current model, the SiC particles are assumed to be stationary since SiC forms a matrix. Due to the elevation in density and the reduced mass of the filler particles (U_3O_8 or other components produced) during synthesis process, the shrinkage of the filler particles needs to be considered. In our model, it is assumed that the U_3O_8/UO_2 particles shrink once they are converted to the UO_2/UC particles. The gaps between the filler particles and the SiC matrix are thus formed. The filler particle can move in the gap as the result of the pressure change caused by generated gases. The total pressure on each filler particle is related to the gas production rate determined from the reaction rate. The structure of the SiC matrix forms a force to impede the motion of the filler particles. It is assumed that the impedance of the motion is induced by the springs or forces from the neighboring structure. In other words, the filler particle is assumed to sit at the center initially (Fig. 2), and the total force on the filler particle is the summation of all the forces from the neighboring matrix. Without reaction, the forces surrounding the filler particle are at equilibrium.

Two key reactions are considered for the synthesis process. It is assumed that the reaction 1 (R4) occurs when the temperature is above 1200 °C and the reaction 2 (R5) occurs when the temperature is higher than 1400 °C.

$$U_3O_8 \rightarrow \alpha_1 UO_2 + (1 - \alpha_1) P_1 \tag{R4}$$

$$SiC + \alpha_2 UO_2 \rightarrow \alpha_3 UC + \alpha_4 Products + (1 + \alpha_2 - \alpha_3 - \alpha_4) P_2, \tag{R5}$$

where a_1, a_2, a_3 and a_4 are the mass (kg) based stoichmetry constants; P_1 and P_2 represent the volatiles produced from reactions 1 and 2, respectively. It should be noted that the reactions between SiC and U_3O_8 are not known yet, but UC is the product. The detailed reaction kinetics and mechanisms are yet to be established.

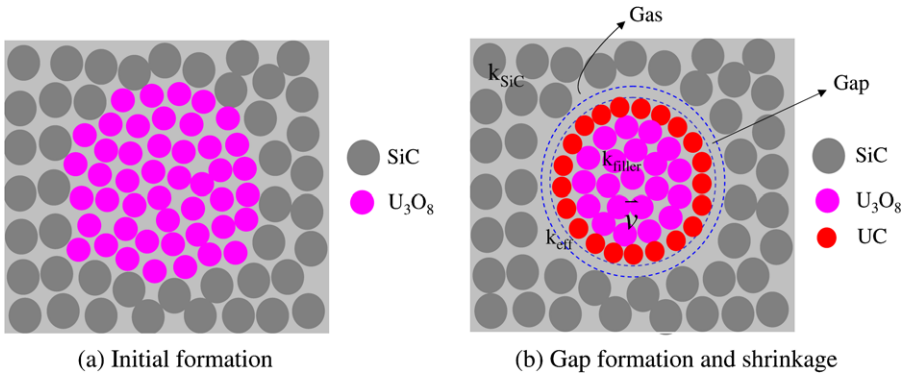

Fig. 2. Models of the shrinkage and movement. k_{filler}, k_{eff} and k_{SiC} are the thermal conductivity of the filler particles, gap and SiC matrix, respectively.

Nevertheless, this paper employs two global reaction steps. Once the detailed reaction kinetics and mechanisms are established in the experiments, the model can be improved.

3. Numerical method

The meshless particle method of SPH was first introduced by Lucy [20] and Gingold and Monaghan [21] to simulate fluid dynamics. Since then, it has been used to model the solidification [22], low Reynolds number flow [23], flow through the porous media [24], immiscible and miscible flows [17,25], etc. In the recent years, the SPH method is applied to study the transport phenomena at the mesoscale, such as the hydrodynamic dispersion [24], the melt flow in the porous structure [27], etc. The SPH method has the advantages in solving the mesoscopic phenomena due to the following reasons. Firstly, it offers a particular suitability to tackle the problems dealing with multi-physics. This is not typically the case with the grid methods. Secondly, it is easy to handle the complex free surface and the material interface. For instance, the particle equivalent of the heat conduction and concentration diffusion equations can be designed so that the discontinuities in the material properties can be handled easily without an explicit reference to the interface between phases [26,28]. The SPH method is thus used here to solve the heat and mass transfer at the particle level [29–31].

3.1. Basic concept of SPH method

In SPH, the entire system is represented by a finite number of particles that carry individual mass and occupy individual space. The governing equations for the fluid flow are written as a set of partial differential equations in the Lagrangian form. The set of the partial differential equations include the mass, momentum, energy, and species conservation. Using the particles as the interpolation points, the Navier–Stokes equations in the Lagrangian form can be discretized into a system of the ordinary differential equations using the kernel and particle approximations [26], which involves approximating the values of functions and derivatives at a particle using the information from all the neighboring particles. With an explicit integration algorithm, the ODEs are solved and the time history of all the field variables is obtained.

3.2. Assumptions

The U_3O_8 filler particles are assumed to disperse in the SiC matrix and both are represented by the SPH particles, as shown in Fig. 1. These SPH particles are assigned a mass, position, density, temperature and concentration of the SiC or filler particles. The SiC particles are assumed to be stationary due to the matrix structure. The U_3O_8 filler particles are allowed to move and also react with the SiC SPH particles. If the temperature of a U_3O_8 SPH particle is above 1200 °C, it will be converted into the UO_2. If the SiC volume ratio in a UO_2 SPH particle is above a critical value and the temperature of the UO_2 SPH particle is above 1400 °C, the UO_2 SPH particle will be converted into the UC particle. The critical concentration value ensures the enough SiC particles being present to synthesize with the UO_2 SPH particles. The governing equations of the mass, heat and concentration are described next.

3.3. SPH equations

The mass conservation equation in the Lagrangian form is written as

$$\frac{D\rho}{Dt} + \rho\nabla\cdot v = \dot{m}. \tag{6}$$

The SPH form of the mass conservation equation is

$$\frac{D\rho_i}{Dt} = -\rho_i \sum_{j=1}^{N} \frac{m_j}{\rho_j} v_{ij}^{\beta}\cdot\frac{\partial W_{ij}}{\partial x_i^{\beta}} + \dot{m}_i, \tag{7}$$

where m_i and ρ_i are the mass and density of the particle i, respectively; W_{ij} is called the kernel function in SPH; β is the coordinate direction; $v_{ij}^{\beta} = (v_i^{\beta} - v_j^{\beta})$.

The energy equation in the Lagrangian form is as follows:

$$\rho c_P \frac{DT}{Dt} = \nabla(k\nabla T) + \dot{Q}. \tag{8}$$

The particle approximation of the energy equation is expressed as:

$$\left(\rho c_p \frac{DT}{Dt}\right)_i = \left(\sum_j \frac{m_j}{\rho_j}(k_j - k_i)\frac{\partial W_{ij}}{\partial x_i^{\beta}}\right)\left(\sum_j \frac{m_j}{\rho_j}(T_j - T_i)\frac{\partial W_{ij}}{\partial x_i^{\beta}}\right) + k_i\sum_j \frac{m_j}{\rho_j}(T_j - T_i)\frac{\partial^2 W_{ij}}{\partial x_i^{\beta}\partial x_i^{\beta}} + \dot{Q}_i. \tag{9}$$

The mass fraction of the SiC is Y and thus the mass of the SiC in a mass M of the medium is YM. The diffusion and reaction of the SiC is given by the following equation [22]:

$$\frac{DY}{Dt} = \frac{1}{\rho}\nabla(D\nabla Y) + \dot{Y}, \tag{10}$$

where D is the diffusion coefficient. The rate of change of the mass fraction Y_i is given by

$$\left(\frac{DY}{Dt}\right)_i = \left(\sum_j \frac{m_j}{\rho_j}(D_j - D_i)\frac{\partial W_{ij}}{\partial x_i^{\beta}}\right)\left(\sum_j \frac{m_j}{\rho_j}(Y_j - Y_i)\frac{\partial W_{ij}}{\partial x_i^{\beta}}\right) + D_i\sum_j \frac{m_j}{\rho_j}(Y_j - Y_i)\frac{\partial^2 W_{ij}}{\partial x_i^{\beta}\partial x_i^{\beta}} + \dot{Y}_i \tag{11}$$

Table 1
Thermophysical properties used in the analysis and modeling.

Parameters	Value used in the model
c_{pg} (J/kg K)	1600
c_{ps} (J/kg K)	1080
k_{s1} (W/m K)	100
k_{s2} (W/m K)	100
k_{gas} (W/m K)	0.1859
ρ_1 (kg/m^3)	8600
ρ_2 (kg/m^3)	2500
ρ_g (kg/m^3)	0.15
D (m^2/s)	4.5×10^{-8}

Note that the diffusion is very weak in this process comparing with reaction.

It is assumed that the heat content of the system only changes because the particles lose or gain heat through the boundary, although it would be possible to include the heat sources such as reaction heating. For the problem considered here, the heat fluxes are obtained from the global model and are applied to the SiC particles at the four boundaries.

Using the standard techniques such as the leapfrog (LF), predictor–corrector and Runge–Kutta (RK) schemes can numerically integrate the ordinary differential equations for the physical variables for every particle. In this paper, the LF method is employed for its low memory storage and efficiency. The particle density, velocity, internal energy and position can be updated with the LF method [26].

3.4. Shrinkage and particle movement

At the beginning, a filler particle generated by many SPH particles is set in the middle of the SiC matrix. As the forces are balanced, the pressure forces acted on the filler particle are calculated from the forces on all SPH filler particles. Due to the heat flux and temperature change during process, the temperature of some portion of the particles will increase, and the SPH particles will react and shrink locally. The pressure forces resulted from the gas products will generate larger forces on the SPH filler particles near the reaction region. The filler particles will then be pushed to move due to the imbalance of the total forces. The movement will continue until reactions are completed. There are two ways to handle the gap. The first method assumes that a small gap exists between the filler particle and the surrounding SiC matrix and the gap contains no material. The SPH particles are pushed away by the gap. The overall density, thermal conductivity and diffusivity will be reduced slightly due to the position changes of the SPH particles. The second method is more complicated. The gas SPH particles are generated and filled into the gap. The gas SPH particles will have their own properties such as mass, thermal conductivity, etc. Both methods are here tested. Since the gap between the filler particles and SiC matrix is usually very small in our cases, e.g., less than 25% of the smoothing length, the results obtained by two methods are almost the same. Using the SPH method, the shrinkage and the movement of the filler particles can be treated straightforward. This is one of the advantages of this method comparing with the grid methods.

4. Results and discussion

The basic thermal and physical properties used in the simulation are listed in Table 1. The dimension of the unit is identical to the macrocell size in the global model (Fig. 1): 0.62 mm × 0.62 mm. The black and grey solid circles represent the SiC and

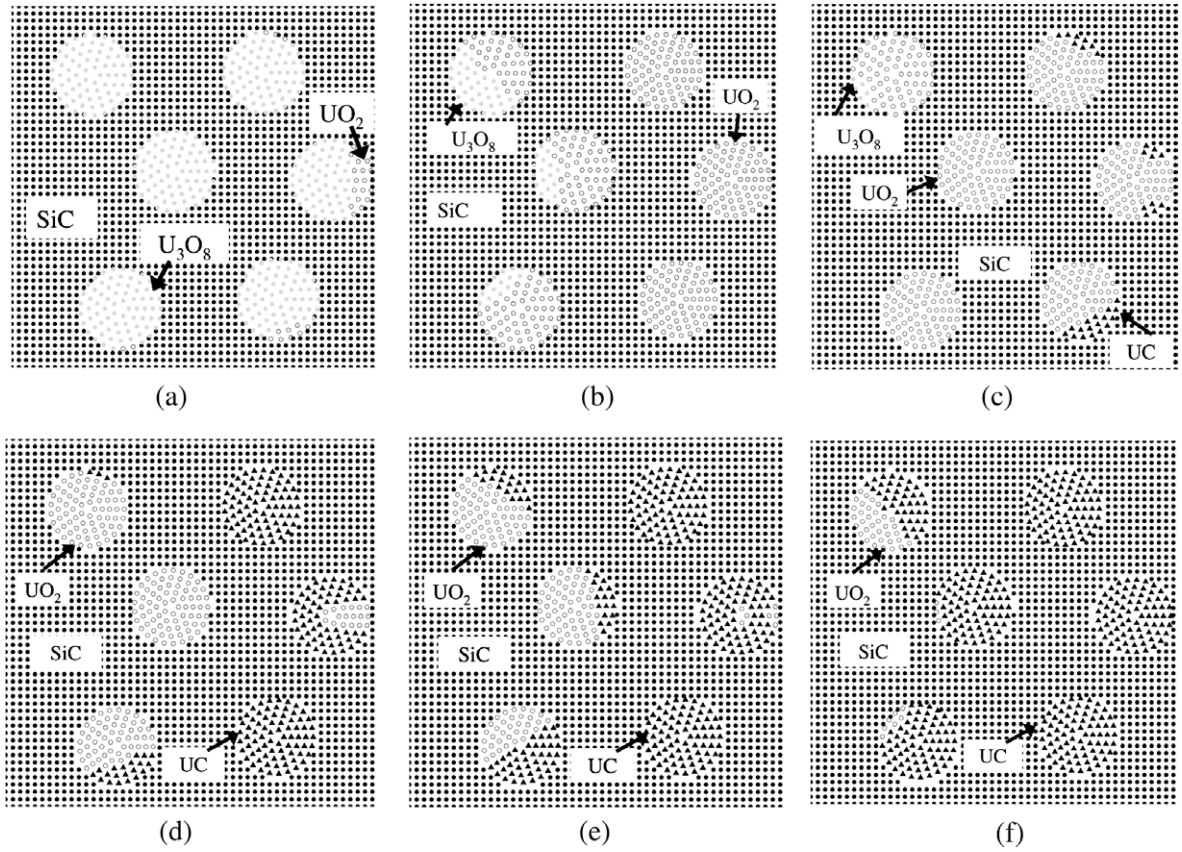

Fig. 3. The structure evolutions of the filler particles for the baseline case. The volume ratio of the filler particles is 20% and the diameter of the filler particles is 0.062 mm. Reaction time is (a) 5.5, (b) 7.0, (c) 8.5, (d) 10, (e) 11.5 and (f) 13 h, respectively. The black solid circle, grey solid circle, black hollow circle and black triangle represent SiC, U_3O_8, UO_2 and UC, respectively.

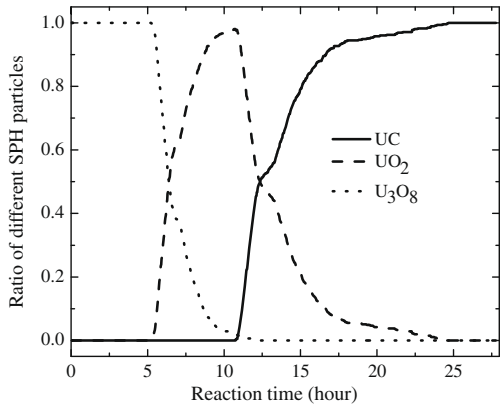

Fig. 4. The composition evolution of filler particles for the baseline case.

U_3O_8 SPH particles, respectively. Four heat fluxes, q_i'' (i = 1, 2, 3 and 4) are computed from the macroscale model and applied to four boundaries. The directions of the heat fluxes are also illustrated. It is noted that the heat fluxes in the x-direction is higher than that in the y-direction. We study the effect of the heating rate, q_i'', applied to the macro computational domain, filler particle volume and size on the evolution of the species and the structures.

4.1. Baseline case study

A baseline case is selected as follows: the volume ratio of the filler particles is 20%, and the filler particle diameter is 0.062 mm. The heating flux applied to the macro computational domain is 0.05 W/m^2. The evolutions of the structure and the composition are presented first. Fig. 3 shows the structure evolution of the filler particles. The black solid circle, grey solid circle, black hollow circle and black triangle represent SiC, U_3O_8, UO_2 and UC, respectively. It is seen that the SPH U_3O_8 particles close to the right and lower boundaries are converted to UO_2 first (Fig. 3a and b), this is where the highest temperature resided as the heat fluxes flow into the domain from the right and lower boundaries. The same reason explains why the UO_2 SPH particles close to the right and lower boundaries are converted to UC first (Fig. 3c–f). Meanwhile, the UO_2 SPH particles close the SiC matrix are converted to UC earlier. It is interesting to notice that some UO_2 SPH particles very close to the right boundary remain unchanged (Fig. 3d and e). This might be due to the fact that less SiC is available there. To quantify the composition evolution of the filler, we plot the ratio of the SPH particles of U_3O_8, UO_2, and UC to all the SPH filler particles (the total number of U_3O_8, UO_2, and UC SPH particles) in Fig. 4. The total number of the UO_2 SPH particles increases first, and then decreases after they react with the SiC. It is illustrated that the UC production rate remains very high from 10 h to 18 h, and decreases drastically after 18 h when less UO_2 is available. Furthermore, the filler particles shrink after all the U_3O_8 SPH particles are converted to UO_2 as shown in Fig. 3b–f. The gap forms between the filler particles and the SiC matrix.

4.2. The motion of filler particle

The filler particles move in the gap and all the SPH particles composing a filler particle move at the same velocity. The motion of the filler particles is driven by the total gas pressure acted on the filler particles from the neighboring SPH particles. We characterize this motion by plotting the position of the center of a filler particle. Fig. 5 shows the velocity vectors of the filler particles in the baseline case. By choosing the initial position of the filler particle as the reference, we compute the relative position of the filler particle. In addition, the relative position is normalized to the dimension of the unit cell, which is 0.62 mm. Fig. 6 shows the normalized relative position of a filler particle with its diameter of 0.062 mm and 0.056 mm, respectively. The filler volume ratio is set to be 20%. The initial position of the filler particle center is (0.27 mm, 0.34 mm). It is seen that the translational velocity in the x-direction is higher than that in the y-direction. This is because the heat flux along the x-direction (0.1 w/m^2) is higher than that along the y-direction (0.025 w/m^2). Thus, the conversion of UO_2 to UC is faster in the x-direction, and more gases are produced, causing the filler particles moving with higher speed in the x-direction. It is also seen that the filler particles with larger radius move slower due to their greater mass compared with small filler particles.

4.3. The effect of heat flux

The effect of the heat flux q'' applied to the macro computational domain on the composition evolution is studied. Fig. 7 shows the history of the ratio of the UO_2 to UC SPH particles for the heat fluxes of 0.025 w/m^2, 0.05 w/m^2 (baseline case) and 0.1 w/m^2. The filler particle diameter is 0.062 mm for all three cases. The filler particles have the same initial distribution as in the baseline case. It is indicated that the production rates of both UO_2 and UC increases as the heat flux increases.

4.4. The effect of filler particle size

The effect of the filler particle size on the composition evolution is studied. Fig. 8 shows the initial distribution of the filler particles

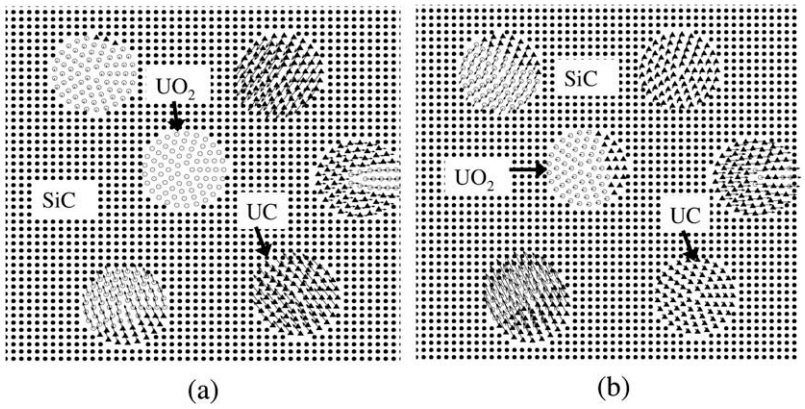

Fig. 5. The velocity vectors of filler particles for the baseline case. The reaction times are (a) 10 h and (b) 11.5 h.

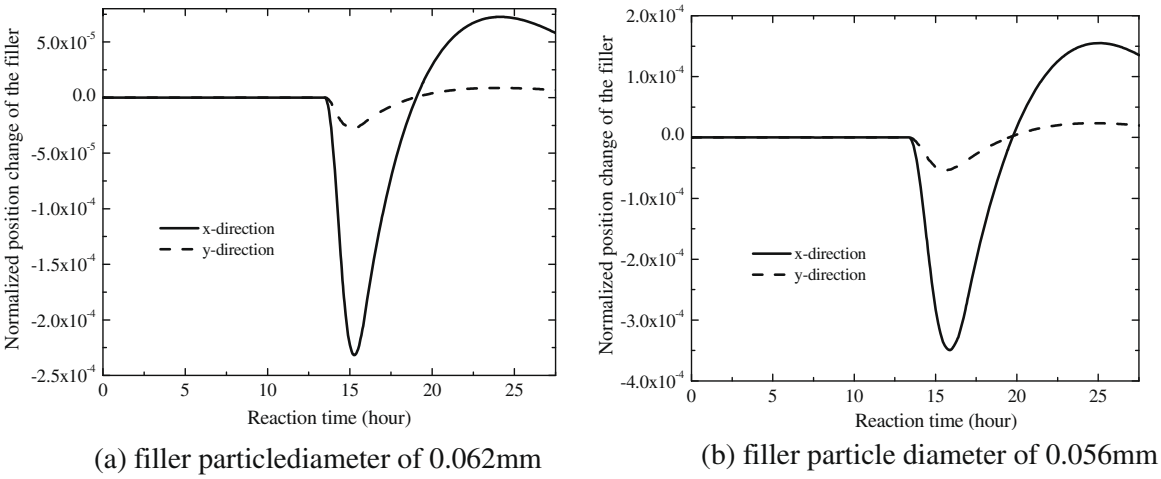

Fig. 6. The normalized relative position of a filler particle.

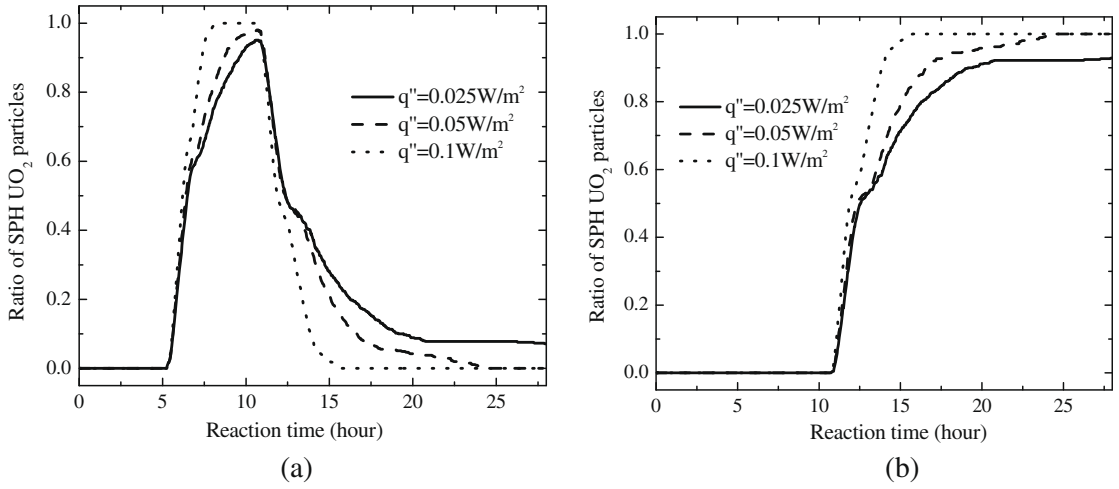

Fig. 7. The composition evolution of filler particles with heat fluxes.

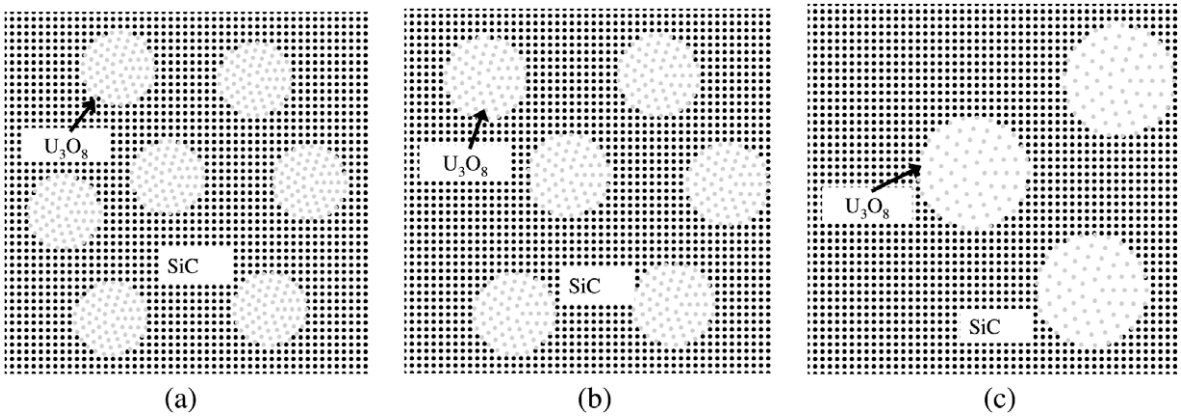

Fig. 8. The initial distribution of filler particles with the diameters of (a) $d = 0.056$ mm and (b) $d = 0.062$ mm and (c) $d = 0.069$ mm. The black solid and grey solid circles represent SiC and U_3O_8, respectively.

with their initial diameters of 0.056, 0.062 (baseline case) and 0.069 mm. The filler volume ratio is assumed to be 20% for all three cases. Fig. 9 shows the history of the ratio of UO_2 to UC SPH particles of three cases. It is indicated that the production rate of the UC increases as the filler particle size increases. This might be explained by the heat flux directions. Another possible reason is that the total gap area associated with the shrinkage of smaller filler particle is larger, making the production rate of UC lower.

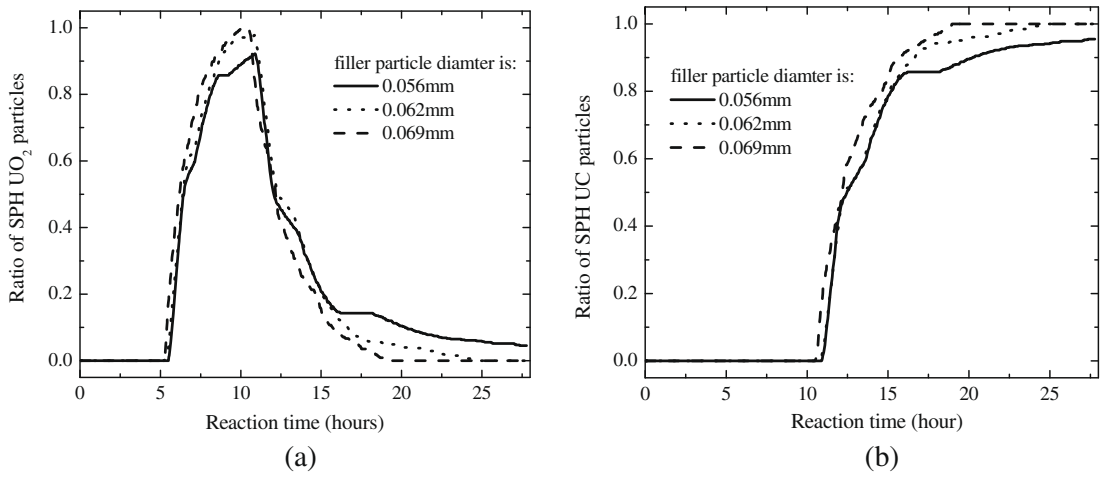

Fig. 9. The composition evolution of filler particles with their sizes: (a) UO_2 and (b) UC.

4.5. The effect of filler particle volume

The effect of filler particle volume on the composition evolution is studied. Fig. 10 shows the initial distribution of the filler particles with three different volume ratios: 10%, 15% and 20% (baseline case). The filler particle diameter is 0.062 mm for all three cases. Fig. 11 shows the history of the ratio of UO_2 to UC SPH particles of three cases. It is indicated that the production rates of both UO_2 and UC increases slightly as the filler particle ratio increases. This might be explained by the heat flux directions. The influence

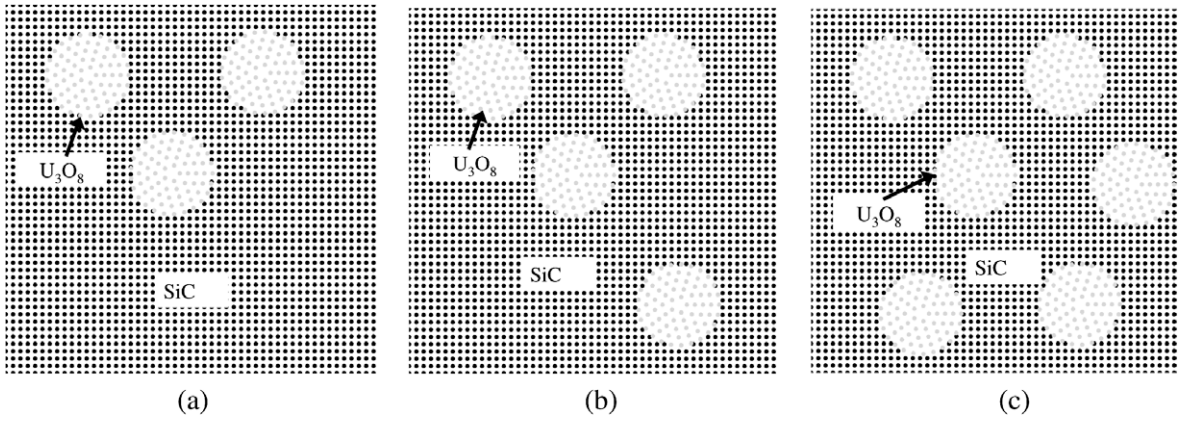

Fig. 10. The initial distribution of filler particles with the volume ratios of (a) $f = 0.1$, (b) $f = 0.15$ and (c) $f = 0.2$. The black solid and grey solid circles represent SiC and U_3O_8, respectively.

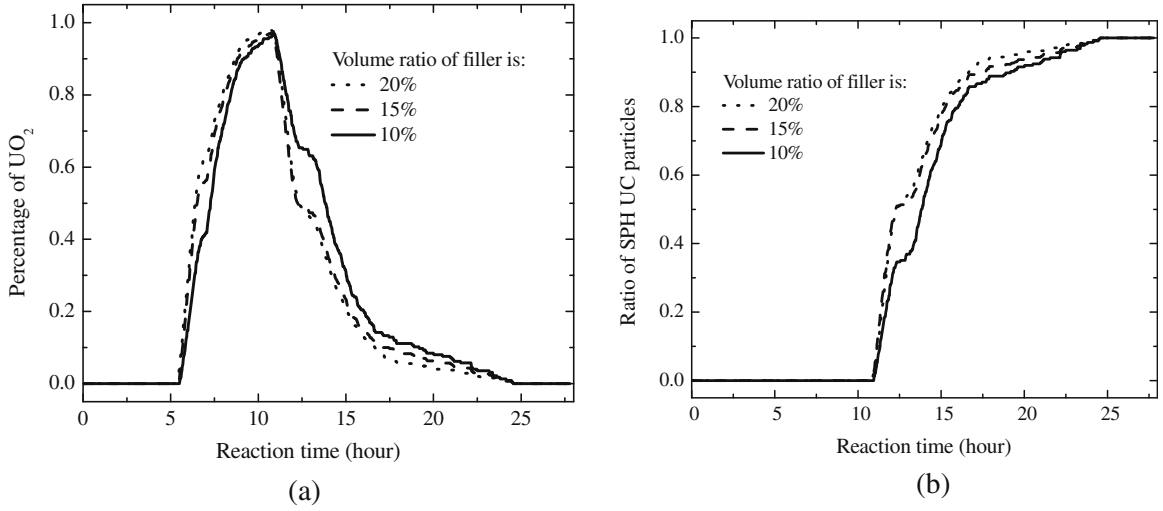

Fig. 11. The composition evolution of filler particles with different volume ratios of filler particles: (a) UO_2, and (b) UC.

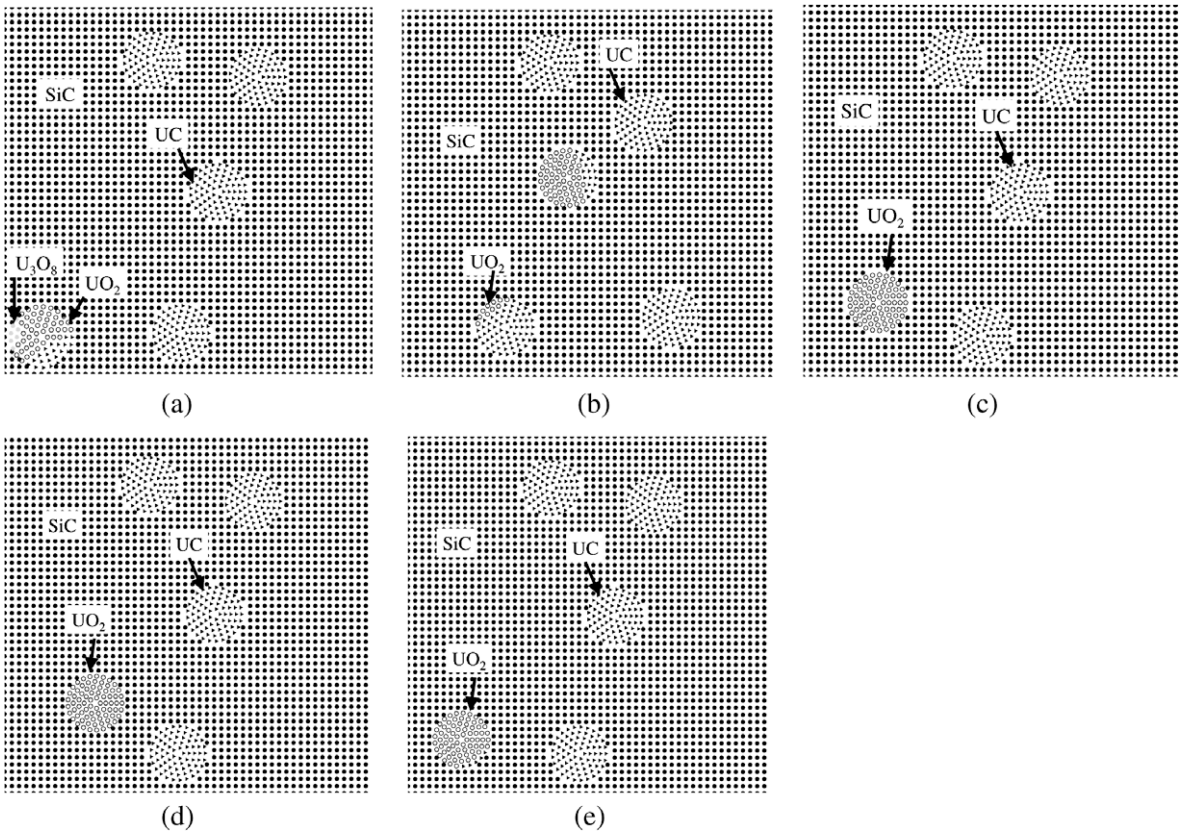

Fig. 12. The structure evolution of filler particles at 10 h for five different distributions, volume ratio of filler particles is 10%: (a) distribution 1, (b) distribution 2, (c) distribution 3, (d) distribution 4 and (e) distribution 5.

of the filler particle volume on the UC production rate is, however, weaker than that of filler particle size when comparing Figs. 9 and 11b. It is interesting to observe that it takes the same reaction time for all SPH filler particles to be converted into the UC particles.

4.6. The effect of particle distribution

With the same particle volume fraction, the material properties will be different if the particle distribution is different. The uncertainty associated with the random distribution of filler particles is studied next. It is characterized by comparing the composition change of filler particles with the same particle size and volume ratio, but different distributions. Five distributions are generated and used to study the uncertainty, as shown in Fig. 12.

Figs. 12–14 show the history of the ratio of UO_2 to UC SPH particles with the given five random distributions of filler particles. The volume ratio of the filler is 10% and 20% in Figs. 13 and 14, respectively. It is found that the distribution of the filler particles will influence the reaction and the composition change of filler particles is more significant if the filler volume ratio is 10%

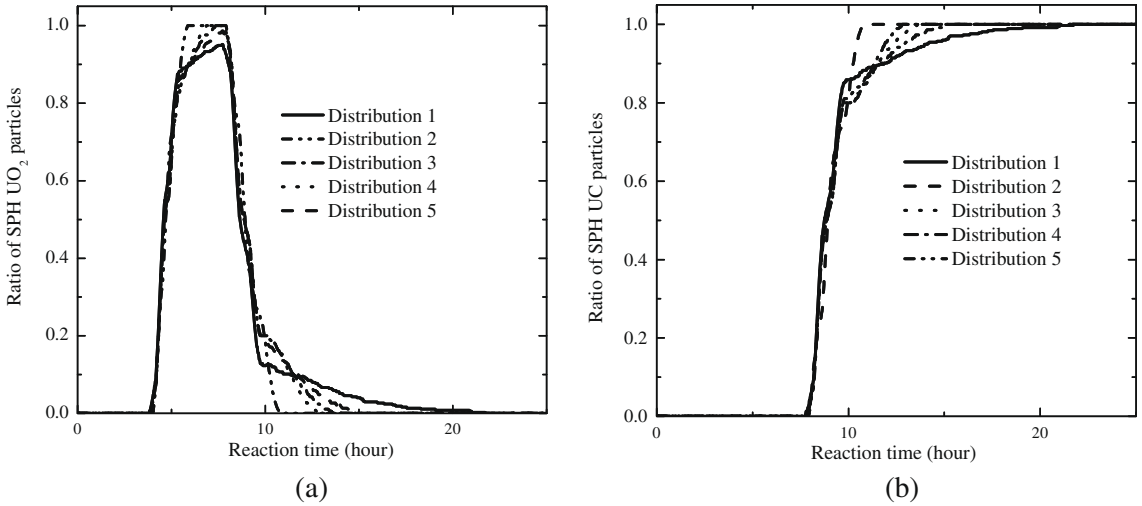

Fig. 13. The composition evolution of filler particles with different distributions for the volume ratio of filler particles of 10%: (a) UO_2 and (b) UC.

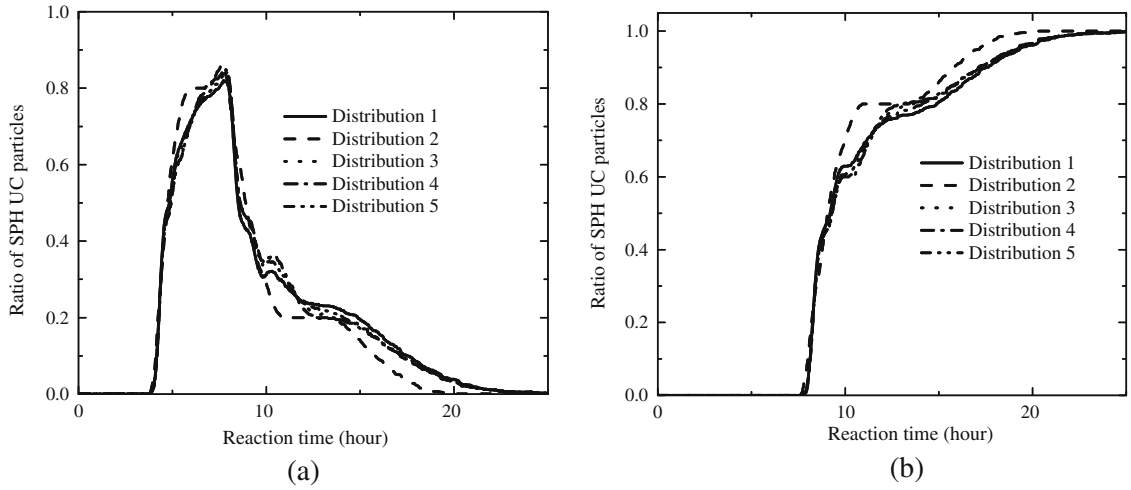

Fig. 14. The composition evolution of filler particles with different distributions for the volume ratio of filler particles 20%: (a) UO_2 and (b) UC.

(Fig. 13). However, this influence becomes weak as the volume ratio reaches 20%. The total reaction time for all SPH filler particles to be converted into UC is about the same for five random distributions when the volume ratio is 20% (Fig. 14).

5. Conclusions

A mesoscopic model based on the smoothed particle hydrodynamics (SPH) method is developed to describe the synthesis of the SiC matrix and uranium oxide particles in a macro-unit. It is the first model, which is capable of considering the synthesis of two different components with solid phases and involving the generation of volatiles at the particle level. Moreover, it can easily handle the geometry changes and shrinkage phenomena. The current work lays the foundation of the application of SPH technique to the solid–solid reaction, in particular, to the problems involved in the synthesis of two components, mass loss, composition change, uniformity of the product and shrinkage, and bulk motion of filler particles in the SiC matrix.

The effects of the filler particle size and volume on species uniformity and structure are investigated using the particle based mesoscopic model. It is concluded that the production rates of both UO_2 and UC increase as the size of the filler particle increases. Furthermore, the production rates of both UO_2 and UC increase as the volume ratio of filler particles increases. The motion of filler particles is also investigated. It is concluded that the particles move with a higher speed in the direction with a higher heat flux and the velocity of the filler particles with a smaller radius is higher. In the future, the mesoscopic model will be integrated with the porous media based macroscopic model so that the material processing can be optimized.

Acknowledgements

We acknowledge the sponsorship from DOE (contract # DE-FC07-05ID14673) and NSF (award # CBET0650604). Hui Zhang and Lili Zheng also acknowledge the financial support from Tsinghua University through the "recruitment of hundreds outstanding scientist" program.

References

[1] A.K. Singh, S.C. Zunjarrao, R.P. Singh, Silicon carbide and uranium oxide based composite fuel preparation using polymer infiltration and pyrolysis, in: 14th International Conference on Nuclear Engineering (ICONE), 2006.
[2] A.A. Solomon, J. Fourcade, S. Lee, S. Kuchibhotla, S. Revankar, R. Latta, P.L. Holman, J.K. McCoy, The polymer impregnation and pyrolysis method for producing enhanced conductivity LWR fuels, in: Proceedings of the 2004 International Meeting on LWR Fuel Performance, Orlando, Florida, American Nuclear Society, La Grange Park, IL 60526, United States, September 19–22, 2004, pp. 146–155. Paper 1028.
[3] T. Hinoki, A. Kohyama, Current status of SiC/SiC composites for nuclear applications, Annales de Chimie: Science des Materiaux 30 (6) (2005) 659–671.
[4] M.Z. Berbon, D.R. Dietrich, D.B. Marshall, D. Hasselman, Transverse thermal conductivity of thin C/SiC composites fabricated by slurry infiltration and pyrolysis, J. Am. Ceram. Soc. 84 (10) (2001) 2229–2234.
[5] Z. Alkan, K. Kugeler, R. Kaulbarsch, C. Manter, Silicon carbide encapsulated fuel pellets for light water reactors, Prog. Nucl. Energy 38 (3–4) (2001) 411–414.
[6] M. Kotani, T. Inoue, A. Kohyama, Y. Katoh, K. Okamura, Effect of SiC particle dispersion on microstructure and mechanical properties of polymer-derived SiC/SiC composite, Mater. Sci. Eng. A 357 (1–2) (2003) 376–385.
[7] Y.W. Lee, S.C. Lee, H.S. Kim, C.Y. Joung, C. Degueldre, Study on the mechanical properties and thermal conductivity of silicon carbide-, zirconia- and magnesia aluminate-based simulated inert matrix nuclear fuel materials after cyclic thermal shock, J. Nucl. Mater. 319 (2003) 15–23.
[8] E. Richter, S. Gramlich, A. Klein, E. Nebauer, I. Rechenberg, U. Zeimer, M. Weyers, Direct growth of GaN on (0001) sapphire by low pressure hydride vapour phase epitaxy, Phys. Status Solidi A 188 (2001) 439–442.
[9] R.M. Tarafdar, T.L. Bergman, Detailed numerical and experimental investigation of non-isothermal sintering of amorphous polymer material, J. Heat Transfer 124 (2002) 553–563.
[10] T. Chen, Y. Zhang, A partial shrinkage model for selective laser sintering of a two-component metal powder layer, Int. J. Heat Mass Transfer 49 (7–8) (2006) 1489–1492.
[11] B. Xiao, Y. Zhang, Analysis of melting of alloy powder bed with constant heat flux, Int. J. Heat Mass Transfer 50 (11–12) (2007) 2161–2169.
[12] Q. He, F. Winter, J.D. Lu, Analysis of the heat transfer mechanism in high-temperature circulating fluidized beds by a numerical model, J. Heat Transfer 124 (2002) 34–39.
[13] P. Kaushal, T. Proll, H. Hofbauer, Model development and validation: co-combustion of residual char, gases and volatile fuels in the fast fluidized combustion chamber of a dual fluidized bed biomass gasifier, Fuel 88 (17–18) (2007) 2687–2695.
[14] A. Jagota, P.R. Dawson, Micromechanical modeling of powder compacts-I: unit problems for sintering and traction induced deformation, Acta Metall. 36 (1988) 2551–2561.
[15] J.I. Martinez-Herrera, J.J. Derby, Analysis of capillary-driven viscous flows during the sintering of ceramic powders, J. AIChE 40 (1994) 1794–1803.
[16] W.M. Gao, L.X. Kong, P.D. Hodgson, Computational simulation of gas flow and heat transfer near an immersed object in fluidized beds, Adv. Eng. Software 38 (11–12) (2007) 826–834.
[17] A.M. Tartakovsky, P. Meakin, Pore scale modeling of immiscible and miscible fluid flows using smoothed particle hydrodynamics, Adv. Water Resour. 29 (10) (2006) 1464–1478.
[18] A.M. Tartakovsky, P. Meakin, T.D. Scheibe, R.M. Eichler West, Simulations of reactive transport and precipitation with smoothed particle hydrodynamics, J. Comp. Physiol. 222 (2) (2007) 654–672.
[19] X. Wang, S. Zunjarrao, H. Zhang, R. Singh, Advanced process model for polymer pyrolysis and uranium ceramic material processing, ICONE14-89099, in: Proceedings of ICONE14, International Conference on Nuclear Engineering, Miami, Florida, 2006.
[20] L.B. Lucy, Numerical approach to the testing of the fission hypothesis, Astronom J. 82 (1977) 1013.

[21] R.A. Gingold, J.J. Monaghan, Smoothed particle hydrodynamics: theory and application to non-spherical stars, Mon. Not. R. Astronom. Soc. 181 (1977) 375.
[22] J.J. Monaghan, H.E. Huppert, M.G. Worster, Solidification using smoothed particle hydrodynamics, J. Comp. Physiol. 206 (2) (2005) 684–705.
[23] J.P. Morris, P.J. Fox, Y. Zhu, Modeling low reynolds number incompressible flows using SPH, J. Comp. Physiol. 136 (1) (1997) 214–226.
[24] Y. Zhu, P.J. Fox, J.P. Morris, A pore-scale numerical model for flow through porous media, Int. J. Num. Anal. Methods Geomech. 23 (9) (1999) 881–904.
[25] A.M. Tartakovsky, P. Meakin, A smoothed particle hydrodynamics model for miscible flow in three-dimensional fractures and the two-dimensional Rayleigh–Taylor instability, J. Comp. Physiol. 207 (2) (2005) 610–624.
[26] G.R. Liu, M.B. Liu, Smoothed Particle Hydrodynamics, A meshfree Particle Method, World Scientific Publishing Co. Pvt. Ltd., 2003.
[27] J.P. Morris, Y. Zhu, P.J. Fox, Parallel simulations of pore-scale flow through porous media, Comput. Geotech. 25 (4) (1999) 227–246.
[28] M.Y. Zhang, H. Zhang, L.L. Zheng, Application of smoothed particle hydrodynamics method on free surface and solidification problems, Num. Heat Transfer A: Appl. 52 (2007) 299–314.
[29] H.S. Fang, K. Bao, J.A. Wei, H. Zhang, E.H. Wu, L.L. Zheng, Simulations of droplet impact and solidification using an improved SPH model, Num. Heat Transfer, Part A 55 (2009) 124–143.
[30] M.Y. Zhang, H. Zhang, L.L. Zheng, Simulation of droplet spreading, splashing and solidification using smoothed particle hydrodynamics method, Int. J. Heat Mass Transfer 51 (2008) 3410–3419.
[31] X.L. Wang, H. Zhang, L.L. Zheng, Novel modeling tool for fixed-bed biomass gasification using high temperature air, J. Ind. Eng. Chem. Res. 46 (2007) 8852–8856.